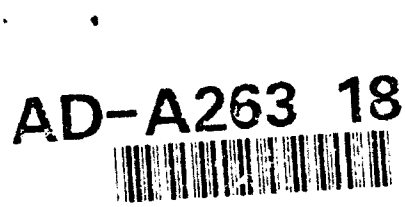

ARMY RESEARCH LABORATORY

Explosive Consolidation of Combustion Synthesized TiC and TiB_2: Precursor Morphology Effects

Laszlo J. Kecskes
Andrus Niiler
Thomas Kottke
Sharon H. Robinson
Frederick B. Pierce

ARL-TR-107 April 1993

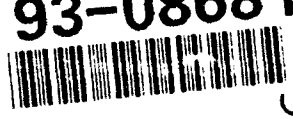

NOTICES

Destroy this report when it is no longer needed. DO NOT return it to the originator.

Additional copies of this report may be obtained from the National Technical Information Service, U.S. Department of Commerce, 5285 Port Royal Road, Springfield, VA 22161.

The findings of this report are not to be construed as an official Department of the Army position, unless so designated by other authorized documents.

The use of trade names or manufacturers' names in this report does not constitute indorsement of any commercial product.

REPORT DOCUMENTATION PAGE

Form Approved
OMB No. 0704-0188

1. AGENCY USE ONLY (Leave blank)	2. REPORT DATE	3. REPORT TYPE AND DATES COVERED
	April 1993	Final, 1 Oct 87 - 1 Oct 89

4. TITLE AND SUBTITLE

Explosive Consolidation of Combustion Synthesized TiC and TiB_2: Precursor Morphology Effects

5. FUNDING NUMBERS

PR: 1L161102AH43
WU: 61102A

6. AUTHOR(S)

Laszlo J. Kecskes, Andrus Niiler, Thomas Kottke, Sharon H. Robinson, and Frederick B. Pierce

7. PERFORMING ORGANIZATION NAME(S) AND ADDRESS(ES)

U.S. Army Research Laboratory
ATTN: AMSRL-WT-WD
Aberdeen Proving Ground, MD 21005-5066

8. PERFORMING ORGANIZATION REPORT NUMBER

9. SPONSORING/MONITORING AGENCY NAME(S) AND ADDRESS(ES)

U.S. Army Research Laboratory
ATTN: AMSRL-OP-CI-B (Tech Lib)
Aberdeen Proving Ground, MD 21005-5066

10. SPONSORING/MONITORING AGENCY REPORT NUMBER

ARL-TR-107

11. SUPPLEMENTARY NOTES

12a. DISTRIBUTION/AVAILABILITY STATEMENT

Approved for public release; distribution is unlimited.

12b. DISTRIBUTION CODE

13. ABSTRACT *(Maximum 200 words)*

The combustion synthesis/dynamic consolidation (CS/DC) technique has been applied to titanium-carbon and titanium-boron mixtures with different initial precursor carbon and boron powder morphologies. The evolution of the CS/DC product structure was investigated by analyzing and comparing the combustion synthesis products following three fabrication process steps: reacted loose powders, reacted green compacts, and reacted green compacts which were dynamically consolidated shortly after the synthesis. In all cases, the purity of the precursor carbon and boron powders was found to affect the products' residual porosity. However, the dependence of the resultant product grain morphology on the precursors' morphology was not as straightforward. Correlations between the respective product structures and possible reaction mechanisms are discussed.

14. SUBJECT TERMS

SHS, combustion synthesis, explosive compaction, dynamic consolidation, TiC, TiB_2, precursors, morphology, processing, reaction mechanism

15. NUMBER OF PAGES

37

16. PRICE CODE

17. SECURITY CLASSIFICATION OF REPORT	18. SECURITY CLASSIFICATION OF THIS PAGE	19. SECURITY CLASSIFICATION OF ABSTRACT	20. LIMITATION OF ABSTRACT
UNCLASSIFIED	UNCLASSIFIED	UNCLASSIFIED	UL

INTENTICNALLY LEFT BLANK.

TABLE OF CONTENTS

INTENTIONALLY LEFT BLANK.

LIST OF FIGURES

LIST OF TABLES

INTENTIONALLY LEFT BLANK.

ACKNOWLEDGMENTS

The authors would like to express their gratitude to Messrs. Ralph F. Benck and Paul H. Netherwood for their assistance in some of the experiments.

INTENTIONALLY LEFT BLANK.

1. INTRODUCTION

At the U.S. Army Research Laboratory, the Combustion Synthesis/Dynamic Consolidation technique (CS/DC) has been applied to fabricate titanium carbide and titanium diboride (Niiler et al. 1988, 1990). In this technique, two independent processes, Combustion Synthesis (CS) and Dynamic Compaction (DC), are successfully combined into a two-step process to fabricate high- to full-density ceramics from powdered precursors. First, an exothermic CS wave is propagated through a green compact made from the powdered precursors, leaving a porous product at high temperatures. Second, the hot product, contained in a suitable fixture which provides both insulation and strength, is consolidated and its porosity reduced or eliminated by a pressure wave generated by the detonation of a high-explosive charge.

Previous efforts of Niiler (Niiler et al. 1988) and co-workers (Kecskes et al. 1990b) have elucidated both the advantages and disadvantages of fabricating ceramics by CS followed by DC. The series of experiments in the former (Niiler et al. 1988) have established the requirements for successful reaction and compaction of TiC and TiB_2. These included detailed descriptions of the reaction and explosive fixtures, the identification of the critical parameters specifying the ideal consolidation conditions, and a cursory fabrication cost analysis as well. The focus of the latter work was primarily directed to improve the TiC and TiB_2 product characteristics by a more careful examination of the nature, relationship, and type of precursors and the extent of their effects on the product microstructures.

By comparing the features of reaction products obtained from three key steps of the process, this report provides one additional insight into the evolution of the product microstructures obtained during the CS/DC process. In the first step, loose reactant powder mixtures were ignited in a closed container which allowed the free, unconstrained expansion of the CS products. The products of this step will be referred to as Combustion Synthesized, Free (CSF). In the second step, the precursor powders were cold pressed into green compacts which were reacted in the fixture described in Niiler et al. (1988) and allowed to cool slowly to ambient temperature. These second step experiments yielded information on the effect of the containment and thermal insulation provided by the fixture. These products will be referred to as Combustion Synthesized, Contained (CSC), throughout the report. In the third step, a green compact identical to that used in the second experiment was reacted in the fixture and, at the completion of the CS reaction, the hot product was dynamically consolidated. A comparison of these samples to the CSC samples provided insight into how the product structure and morphology evolve during consolidation. The

products from this third step will be referred to as Combustion Synthesized/Dynamically Consolidated (CSDC).

In the following sections, pertinent results from the three steps will be discussed. Specifically, attention will be focused on how the use of different precursors affects structure development and reaction mechanisms in the combustion synthesized and dynamically compacted TiC and TiB_2. Finally, inferences regarding the advantages and limitations of this processing technique will be drawn.

2. EXPERIMENTAL PROCEDURE

Several types of precursor powders with different morphologies and purities were evaluated in terms of their effects on the product microstructure. These powders are described in Table 1. Three types of carbon and two types of boron were used. The carbon powders were graphite, carbon black, and carbon fibers while the boron powders were amorphous and crystalline. All of the powders were examined with Scanning Electron Microscopy (SEM) and Energy Dispersive X-ray Spectroscopy (EDS) to characterize their morphologies and impurity levels.

The titanium-boron and titanium-carbon powders were dry mixed and ball milled for several hours under argon atmosphere. The powder mixtures were uniaxially pressed into 50-mm-diameter by 30-mm-thick, disk-shaped, green compacts. The applied pressure was 40–50 MPa for the titanium-carbon mixtures, and 120 MPa for the titanium-boron mixtures. For the TiC samples, a C/Ti atom ratio of 0.8 was maintained while for the TiB_2 samples, a B/Ti atom ratio of 2.0 was used.

In order to prepare the CSF samples (step 1), a small quantity, 10 g or so, of loose powder from each mixture was reacted in air in a 20-cm^3 closed, cylindrical container that allowed the reacting powder to expand freely but prevented excessive post-reaction oxidation of the product. These products were highly friable as they readily crumbled during handling. Due to their large expansion and rapid thermal quench, these products reflect the morphology obtained shortly after the completion of the CS process. Two green compacts of each mixture were prepared. The first compact was reacted in a CS/DC reaction-compaction fixture (Niiler et al. 1988). In this case, the hot, porous reaction product was not compacted, but was allowed to cool to ambient temperature. The reacting green compact in the reaction vessel is spatially confined and therefore constrained from expanding freely. Kottke (Kottke et al. 1990) has shown that this constraint, especially with TiB_2, affects both the reaction dynamics and product morphology. Samples

Table 1. Description of Precursor Powders

Designation	Size[a]	Purity[a]	Description	Manufacturer
Ti-1	−325[b]	99.7	Titanium	Atlantic (1)
Ti-2	−325	99.5	Titanium	Micron Metal (2)
C-1	0.5 μm	99.5	Graphite, Asbury 850	Asbury (3)
C-2	0.02 μm	90.5	Carbon, Monarch 1300, 90.5% fixed C content	Cabot (4)
C-3	2 μm	99.9	Graphite	ConAstro (5)
C-4	7.5 μm	99.0	Carbon, AVCARB PC30G, 760 μm long	Textron (6)
C-4[c]	7.5 μm	99.0	Carbon, AVCARB PC30G, −44 μm long	Textron (6)
B-1	−325	99.5	Boron, cryst.	Atlantic (1)
B-2	5 μm	96.5	Boron, amorph.	ConAstro (5)
B-3	0.07 μm	99.9	Boron, amorph.	Callery (7)

[a] Manufacturer's specified size and purity in %.
[b] −325 mesh is equivalent to particle sizes less than 44 μm.
[c] After in-house processing.

(1) Atlantic Equipment Engineers, Inc., Bergenfield, NJ.
(2) Micron Metals, Inc., Salt Lake City, UT.
(3) The Asbury Graphite Mills Inc., Asbury, NJ.
(4) Cabot Corporation, Boston, MA.
(5) Consolidated Astronautics, Inc., Milwaukee, WI.
(6) Textron Corporation, Lowell, MA.
(7) Callery Chemical Corporation, Pittsburgh, PA.

made by this procedure were designated CSCs (step 2). These samples usually expanded during the reaction to fill the reaction fixture cavity and, consequently, were approximately 30 mm thick and 50–52 mm in diameter. However, it may be noted that, because of the violence of the CS reaction, in some of the TiB_2 samples only about 70% of the initial green compact mass was retained. The second compact was reacted in an identical fixture and, at the cessation of the reaction, the product was consolidated into a dense ceramic by the action of an explosive charge. To produce nearly full density TiC and TiB_2 samples, c/m values (explosive charge mass to compression plate mass ratio) of 0.44 and 0.22 were used, respectively. These c/m values were selected based on the experiments described in Niiler et al. (1988) to optimize sample densities without producing excessive cracking. The experimental procedures have been described at length in the above reference. These CSDC samples (step 3) were approximately 12 mm thick with a diameter of 50 mm. With this procedure, each CSDC and CSC product could be directly compared to the CSF morphology as well as that of the precursor powders.

Because the CSF and the CSC products retained at least 50% porosity, they were vacuum impregnated with epoxy before being sectioned with a diamond cut-off saw and polished. Flat sections from the core region of the CSDC samples, cut in an Electric Discharge Machine, were also mounted in a glass-fiber reinforced thermosetting diallyl-phthalate resin compound and polished. Due to their extreme hardness, all of the TiC and TiB_2 ceramics necessitated the exclusive use of diamond products during the polishing procedure. In the usual sequence, the samples were first coarse ground until plane, then fine polished with successively finer diamond sprays to a 1/4-μm finish. Fracture surfaces were produced by impact loading the CSC and CSDC samples. The polished cross sections and fracture surfaces from the CSC and CSDC samples were examined with SEM and EDS for grain morphology, structure, and intergrain bonding. In the case of the CSDC samples, the microscopic evaluation was followed by microhardness measurements. Hardness measurements were performed at room temperature using a Knoop indenter with both 100-g and 400-g test loads. The reported hardness values are averages from a minimum of 15 individual measurements. After the hardness measurements, the polished CSDC sample cross sections were etched for grain size measurements. The etchant for TiC was a mixture of 1 part (by vol.) of concentrated HNO_3, 1 part concentrated HF, and 1 part distilled H_2O. The etchant for TiB_2 was a mixture of 10 parts (by vol.) concentrated HCl and 1 part concentrated HNO_3. The polished samples were etched until their grain structure was clearly evident. The etching time for each sample varied from 30 seconds to several minutes.

After etching, representative optical micrographs of the samples were taken at a magnification of 500X. Rather than using the intercept method, the grain size of the samples was measured directly from the micrographs using a computerized scanning device. To obtain a meaningful average grain size, between 80 and 275 grains were measured from each sample. The area of the grains was measured using Summagraphics® scanning equipment and software. In particular, a digitizing scanner was used to trace the outline of each grain. The area of each traced region was then calculated automatically. A spreadsheet function was used to convert the area found from the micrographs into the area in square micrometers.

3. RESULTS AND DISCUSSION

3.1 Titanium-Carbon System. Table 1 summarizes the sizes and purities of the titanium and carbon precursor powders as listed in the manufacturer's specifications. The first sample was made with the C-1 graphite, the second sample with the C-2 carbon black, and the third sample with a 50/50 at.% of the C-3 graphite and the C-4 carbon fibers. All of these samples were prepared with the Ti-1 titanium. A fourth sample was also made with the C-3 and C-4 mixture. In this case, however, another titanium, Ti-2, was used. The primary reason for the use of the mixture of graphite and fibers was that green compacts made with carbon fibers alone would not hold together during preparation and handling. C-3 graphite, being a larger particle size graphite than C-1, was used because it was expected to minimize the size mismatch between the graphite and fiber precursors.

A special technique was developed to reduce the length of the carbon fibers. As-received TEXTRON carbon fibers, titanium, and graphite powders were premixed by hand, primarily to break up the fiber bundles, but also to distribute them fairly uniformly in the powder mixture. The powder mixture was then uniaxially compressed at approximately 20 MPa. Under the applied stress, the long and relatively brittle fibers buckled and fractured when bent around the smaller titanium particles. With repeated cycles, this "fiber crushing technique" was quite successful in reducing the length of the fibers from their as-received 0.76 mm (760 μm) to a length of about 50 μm (equivalent to −325 mesh), or less.

Secondary electron micrographs of the precursor titanium, graphite, and fiber/graphite-titanium mixture are shown in Figure 1. The micrograph of the Ti-1 titanium (Figure 1A) reveals large particles with average dimensions of 20–30 μm. AE titanium (see Table 1) was selected specifically for its high (3 wt.%) contamination with iron to reduce excessive grain growth in the CSDC samples (Niiler et al.

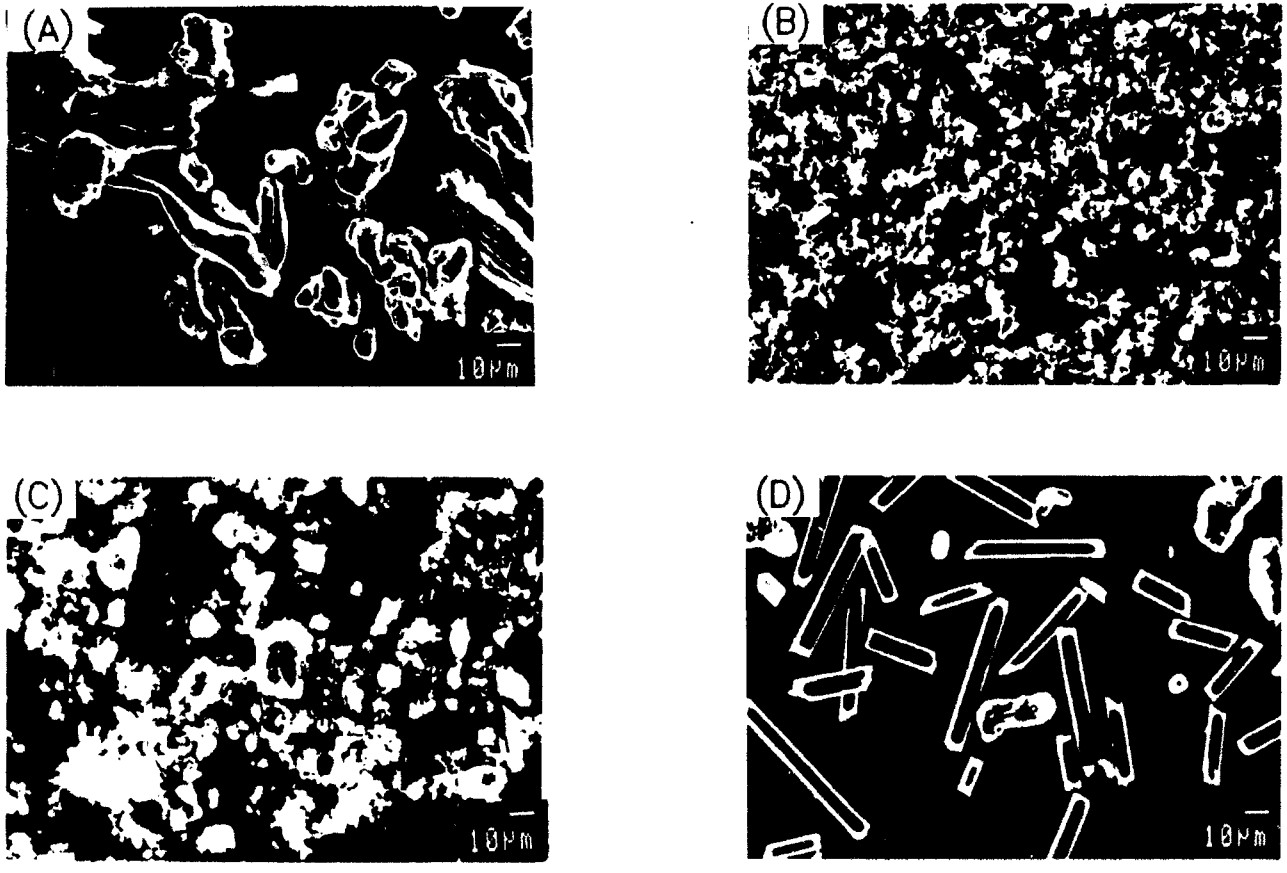

Figure 1. Secondary electron micrographs of the precursor powders with Ti-1 titanium in 1A, C-1 graphite in 1B, C-2 carbon black 1C, and fractured C-4 carbon fibers in the titanium-carbon mixture in 1D.

1988). The C-1 graphite (Figure 1B) is relatively uniform and fine with the flakes about 5–10 μm in diameter and less than 1 μm thick. Though not shown in the figure, the C-3 graphite is similar to C-1, consisting of uniformly flaked particles approximately 15–20 μm in diameter and also less than 1 μm thick. The C-2 carbon black particles (Figure 1C) are extremely small but readily form into 5–20-μm rounded agglomerates due to electrostatic attraction. The C-4 carbon fibers in the fiber/graphite-titanium mixture (Figure 1D) are about 50 μm in length and about 8 μm in diameter. The acicular particles in the figure are titanium. It may be noted that the figure shows a fiber-rich area with the intent to demonstrate a variation in fiber dimensions. That is, while no graphite flakes can be seen in the figure, a 50/50 at.% fiber/graphite ratio exists in the mixture. SEM and EDS analysis of the graphite (C-1 and C-3) and carbon fibers (C-4) detected no impurities, while analysis of the carbon black (C-2) detected the presence of sulfur and chlorine (approximately 1 at.%) (Kecskes and Niiler 1988).

The CSF products were extremely friable. Secondary and backscattered electron images of representative areas of these CSF samples are shown in Figure 2. The product resulting from the reaction of carbon black with titanium resembles the shape, but not the size, of the carbon black agglomerates (Figures 2A and 2D). The particles are coarse and have a rough surface. The product made from the graphite (Figures 2B and 2E) resembles the morphology of the graphite flakes with a somewhat smoother surface. Additionally, as evident in the backscattered electron image (2E), this product, unlike the product with carbon black, contains unreacted graphite flakes. The product resulting from the reaction of the fiber/graphite mixture is the most distinctive. Figures 2C and 2F clearly show features that resemble the precursor carbon fibers. As seen in the figure, these fiber-like structures are actually hollow TiC tubes whose walls have a lizardskin-like appearance. Note the unreacted fibers in the image. The regions between adjacent fiber-like structures result from capillary spreading of molten titanium around the precursor graphite agglomerates. An enlarged secondary electron image of the fiber-like structures is shown in Figure 3. The figure clearly shows that the exterior surface of the TiC tubes consists of a network of equiaxed polycrystals. The significance of this substructure will be discussed later.

The backscattered electron micrographs of polished cross sections of the CSF powdered products, shown in Figure 4, reveal that the equiaxed grain structure present in the fiber/graphite sample is characteristic of all of the samples. The lighter grain boundary regions in all of the samples contain the iron impurity found on the Ti-1 powder. Although Figures 2A and 2D showed that the carbon-based TiC "exoskeletal" particles appeared to be solid, it is evident from Figure 4A that these particles are actually hollow rounded shells lined with 10–15 μm sized equiaxed grains much like the grain morphology of the

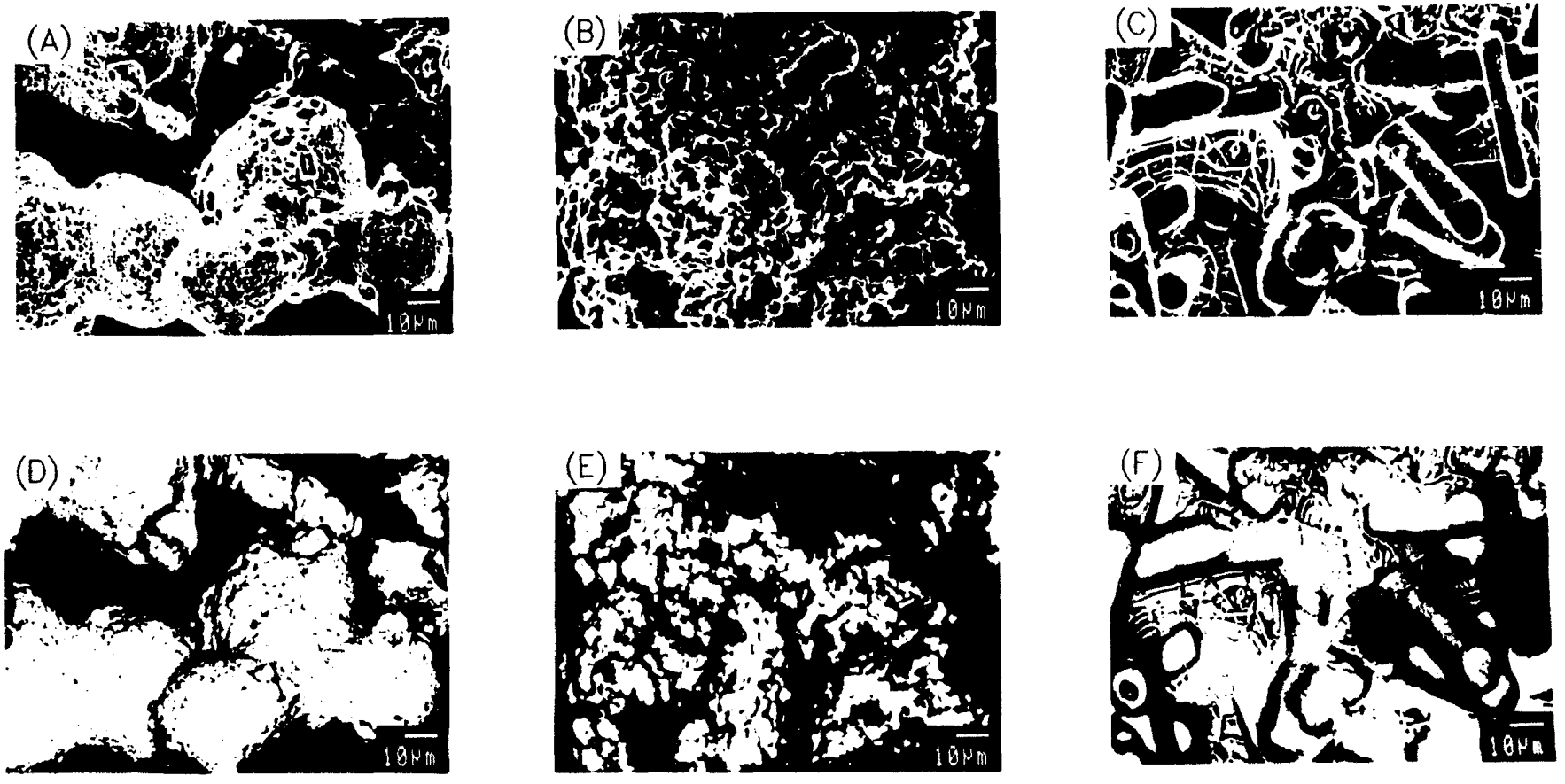

Figure 2. Secondary and backscattered electron images of the CSF TiC products with the carbon black product in 2A and 2D, the graphite product in 2B and 2E, and the fiber/graphite product in 2C and 2F.

Figure 3. Secondary electron micrograph of a fiber-like structure in the CSF fiber/graphite product.

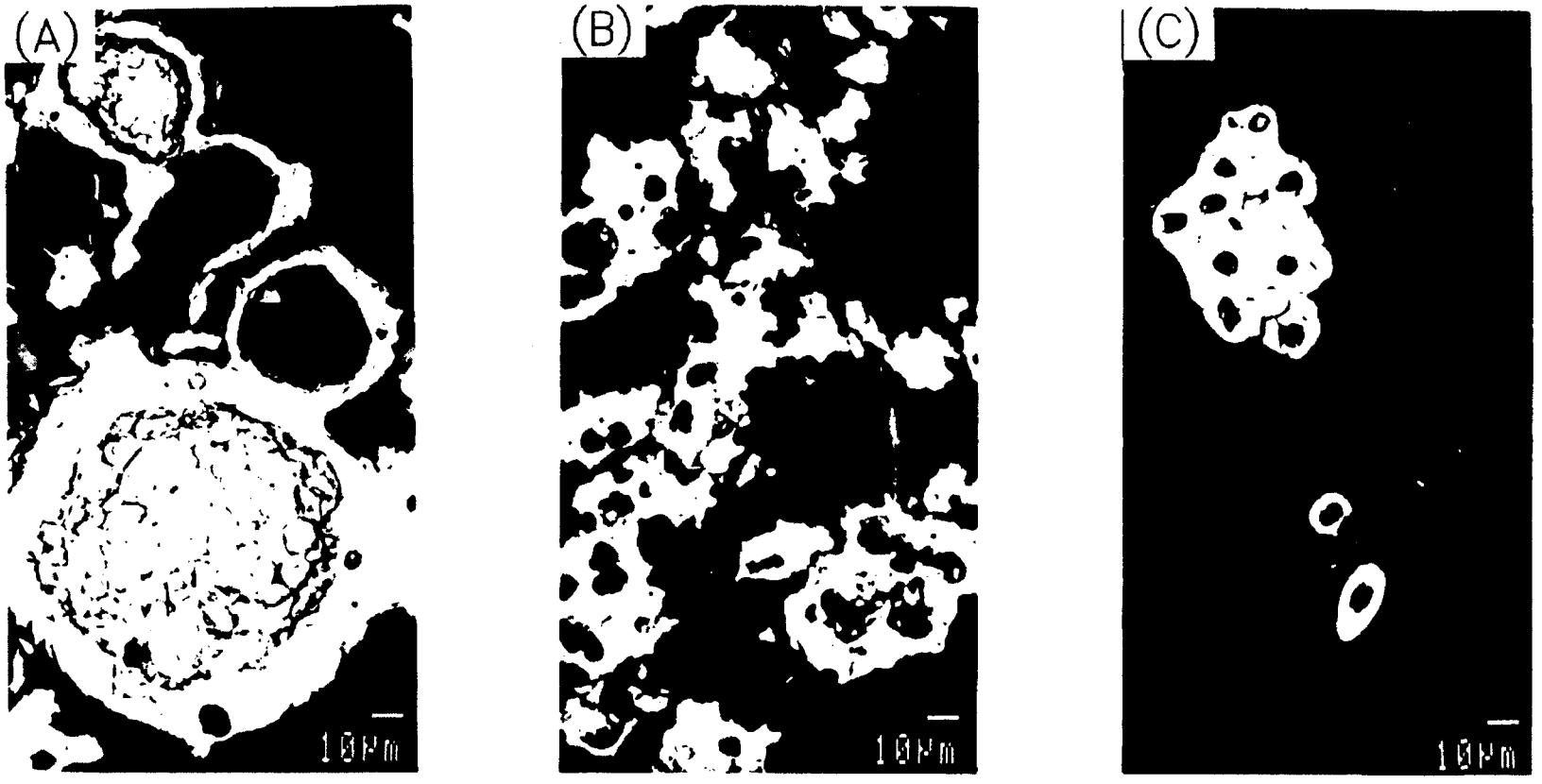

Figure 4. Backscattered electron micrographs of polished cross sections of the CSF powdered TiC products. The carbon black sample is shown in 4A, graphite sample in 4B, and the fiber/graphite sample in 4C.

fiber/graphite samples which were shown in Figures 2C, 2F and 3. The same sized equiaxed grain structure can also be seen in the graphite-based sample (see Figure 4B). In this case, the exoskeletal structures consist of randomly oriented and bonded grains, heavily intermixed with open porosity. Similar results can be seen in Figure 4C, where the cross sections of the hollow TiC tubes confirm the features of Figures 3, 2C, and 2F. Note how the equiaxed grains lining the tube wall maintain a fairly round cavity.

The CSC TiC samples, i.e., those reacted in the CS/DC fixture but not consolidated, were also examined in the SEM. Backscattered electron images of polished and fracture surfaces of these CSC samples are shown in Figure 5. The graphite sample is shown in Figures 5A and 5D, the carbon black sample in Figures 5B and 5E, and the fiber/graphite sample in Figures 5C and 5F. The morphologies of the CSC samples are less distinct and generally consist of the equiaxed, rounded 10–15 μm grains interspersed with 50% open porosity. The grain size of these samples and those found in the lining of the "exoskeletal" structures of the CSF samples are approximately the same. No evidence of the CSF exoskeletal structures could be found in either the carbon black or graphite samples. In contrast, some features of the fiber/graphite sample can be linked with those in the CSF sample. The porosity is markedly different from that seen in the other two samples. About half of the porosity is small and rounded, similar to that found in the sample with graphite. The remaining pores are elongated with a uniform diameter. From their shape, it can be inferred that the elongated pores are caused by the presence of long carbon fibers. Nevertheless, as apparent from the remaining figures with smaller carbon precursors, the features of the CSC samples become less distinct. That is, the constraining effect of the reaction fixture greatly reduces the impact of the precursor carbon morphology on the CSC product morphology.

As revealed by the polished and fracture surface micrographs in Figure 6, the CSDC TiC microstructures consist of equiaxed, rounded, or faceted grains which are interspersed with closed porosity. The residual porosity, usually found at grain triple junctions, appears to scale with the grain size. The TiC sample made with carbon black, Figures 6B and 6E, appears to have lower net porosities than those made with graphite, Figures 6A and 6D, and fiber/graphite, Figures 6C and 6F. As shown in Table 2, no clear correlation could be found between the morphology and size of the precursor carbon agglomerates or individual graphite or fiber particles and that of the CSDC TiC samples. Fractographs of the samples included in Figure 6 reveal a mixed intergranular and transgranular failure mode. Results of the TiC microhardness measurements of the samples are listed in Table 3. As is evident from fracture surface characteristics and microhardness values, the microhardness of all the CSDC TiC samples is similar.

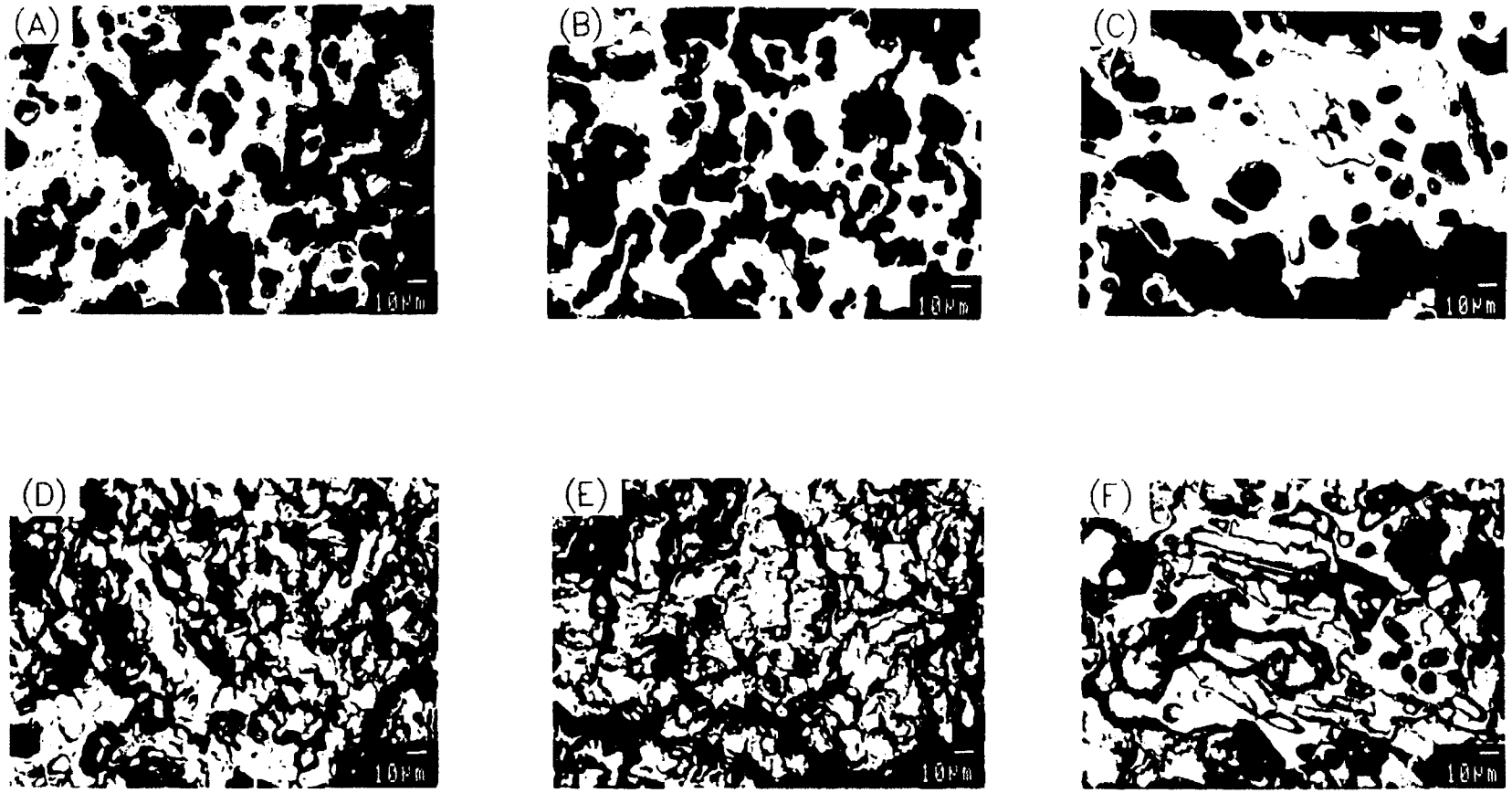

Figure 5. Polished and fracture surfaces of the CSC TiC samples. The graphite sample is shown in 5A and 5D, the carbon black sample in 5B and 5E, and the fiber/graphite sample in 5C and 5F.

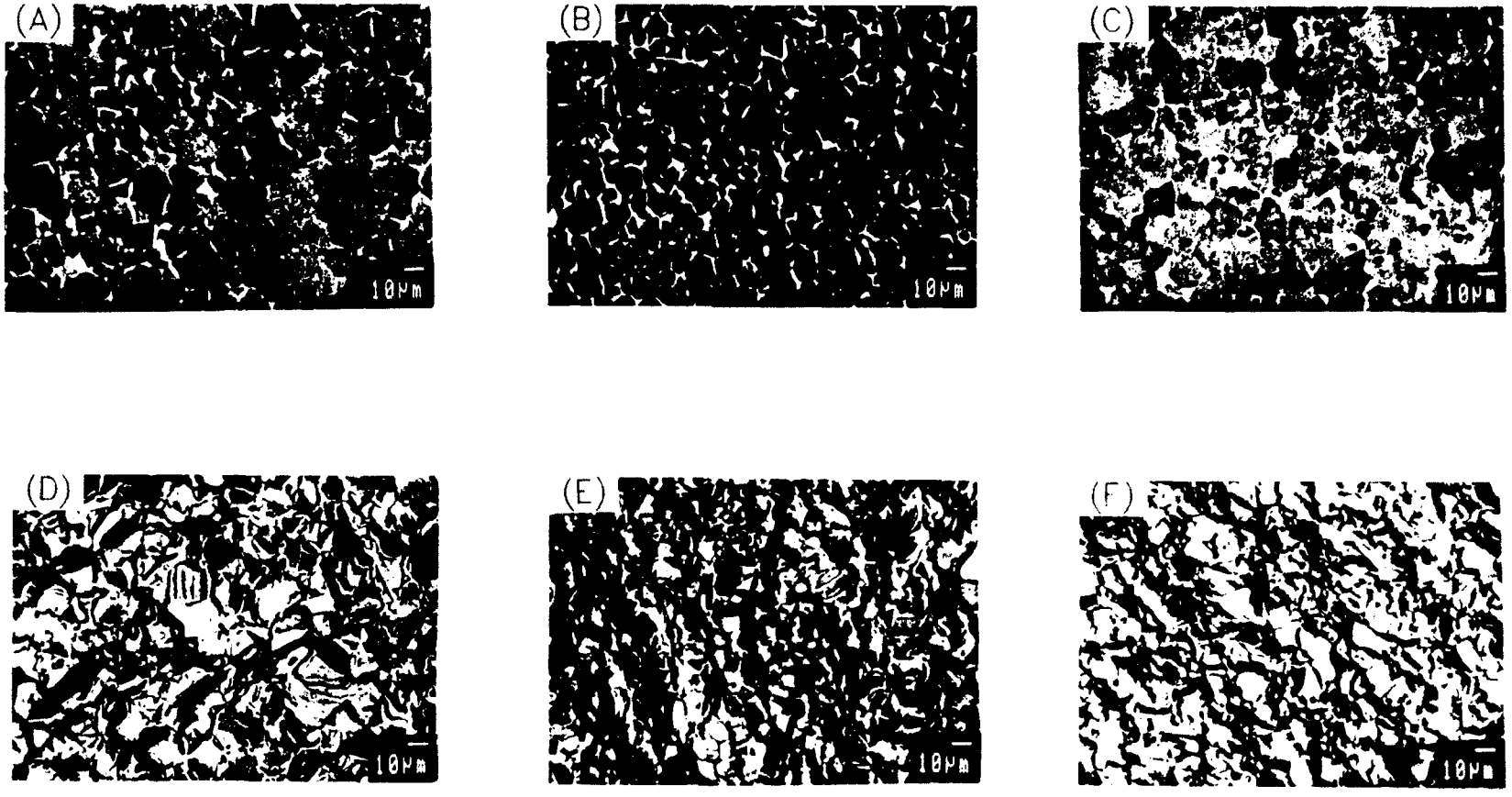

Figure 6. Polished and fracture surfaces of the CSDC TiC samples. The graphite sample is shown in 6A and 6D, the carbon black sample in 6B and 6E, and the fiber/graphite sample in 6C and 6F.

Table 2. TiC Sample Grain Size

Sample	Precursors		No. of Grains	Grain Area, (μm^2)
TiC-1	Ti-1	C-1	244	220.0
TiC-2	Ti-1	C-2	272	80.0
TiC-3	Ti-1	C-3/C-4[a]	228	120.0
TiC-4	Ti-2	C-3/C-4[a]	83	560.0

[a] After in-house processing. See Table 1.

Table 3. TiC Sample Microhardness

Sample	Precursors		HK (100 g), (GPa)	HK (400 g), (GPa)
TiC-1	Ti-1	C-1	22.8+/–0.8	16.4+/–0.5
TiC-2	Ti-1	C-2	20.3+/–0.6	15.8+/–0.4
TiC-3	Ti-1	C-3/C-4[a]	20.6+/–0.8	13.6+/–0.3
TiC-4	Ti-2	C-3/C-4[a]	21.4+/–0.5	16.1+/–0.2

[a] After in-house processing. See Table 1.

Previously, it has been shown that the TiC grain size is also strongly affected by impurities found on the precursors (Kecskes et al. 1990a). Coupled with the well-known fact that impurities tend to form hard phases at the grain boundaries, it is believed that the corresponding smaller grain size of the sample with carbon black is predominantly caused by the higher levels of volatile and solid impurities present in the carbon precursor. To verify this hypothesis, an auxiliary experiment was performed to evaluate whether any further grain growth could be achieved in any of the samples. A second 50/50 at.% fiber/graphite-titanium compact was reacted and dynamically consolidated using the same graphite/fiber mixture, but with an iron-free titanium Ti-2. Because of the lack of grain to grain-boundary image contrast in the SEM, the polished cross sections were etched so as to reveal the grain boundaries. Optical micrographs

of the etched samples, TiC with Ti-1 (with Fe) in Figure 7A and TiC with Ti-2 (without Fe) in Figure 7B, indicate a similar, equiaxed grain morphology. The TiC grains with Ti-2 (on the right) are approximately an order of magnitude larger than the TiC grains with Ti-1 (on the left). Therefore, this experiment clearly demonstrates that in the absence of impurities, grain growth can increase dramatically. Conversely, grain size could be controlled by careful adjustment of the amount and type of impurities.

From the physical features of the TiC microstructures presented above, it may be concluded that the CSDC TiC morphology and grain structure is the same in all cases, regardless of the type of carbon precursor. This result is consistent with findings of previous investigators (Niiler et al. 1988, 1990; Dunmead et al. 1989; Mullins and Riley 1989). In the confinement of the CS/DC reaction fixture, the following reaction mechanism could be proposed. As the reaction front propagates through the green compact, the titanium particles are preheated and melt (T_m(Ti) = 1,940 K, T_m = melting point) ahead of the reaction zone. The reaction begins with capillary spreading (Riley and Niiler 1987) and envelopment of the nearby carbon particles by molten Ti. A significant factor in the TiC reaction is the fact that the carbon precursor remains solid (T_{sub}(C) = 3,950 K, T_{sub} = sublimation point) throughout the process. At the titanium-carbon interface, heat is generated as carbon is dissolved into the titanium followed by solid TiC precipitating out of the titanium-rich melt. The observed equiaxed grain structure of the TiC samples is consistent with the dissolution/precipitation mechanism (Dunmead et al. 1989; Mullins and Riley 1989). As demonstrated in the auxiliary experiment, the precipitation mechanism is independent of the presence of iron on the precursor titanium. The major consequence of the iron, or any other dissolved impurity, is to limit grain growth. By forming a eutectic with TiC, iron may also lower the temperature necessary to produce a liquid phase. The unreacted carbon remaining inside the TiC shell most likely is consumed by the action of impurity gases and transported to the titanium through this solid layer (Adachi et al. 1989). As the heat generation process terminates and the reacted TiC begins to cool, the grains forming the shell probably retain their shape due to surface tension. However, in the spatially confining and thermally insulating reaction fixture, these structures will tend to coalesce.

It has been shown that the precursor carbon fingerprint is gradually lost from the CSF powder samples to the CSDC samples. In the context of the reaction process described above, the resultant TiC morphologies can now be explained. Since the heat loss in the CSF powders is quite rapid after the formation of the TiC shell, grain growth is arrested. As a result, the morphology immediately after the reaction is retained. In the CS/DC fixture, however, the more gradual heat loss, coupled with the geometrical constraint of the fixture, causes the exoskeletal particles to adhere to one another, sinter, and form new intergrain bonds. Under some circumstances when the carbon particles are large, some of the

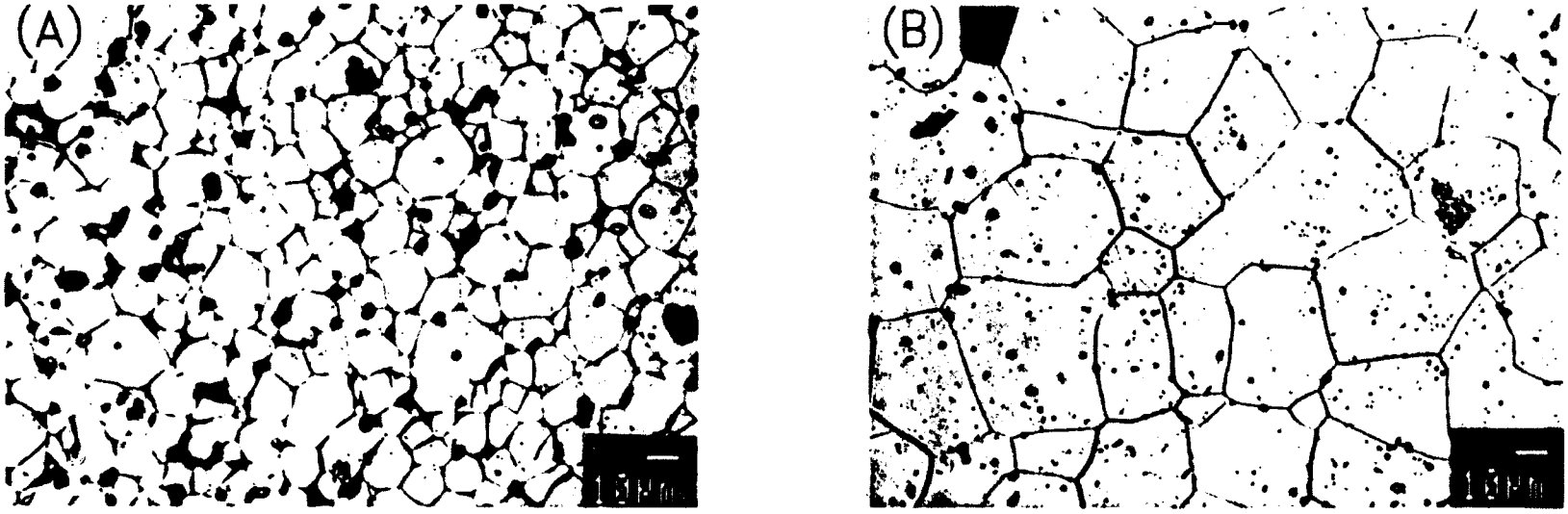

Figure 7. Optical micrographs of etched TiC samples, with Ti-1 (with Fe) in 7A and with Ti-2 (without Fe) in 7B.

CSF pore morphology will be retained. Figures 5 and 6 demonstrate that no significant difference in grain size is observed in the CSC and CSDC samples. Therefore, it may be concluded that the primary function of the consolidation is to close the open porosity. Furthermore, it is believed that the equiaxed grain structure and the roughly identical grain size of the CSDC samples result from the dynamics of the melt/precipitation process. This, in turn, is mainly determined by the insulating properties of the fixture and the reaction kinetics of the TiC system.

3.2 Titanium-Boron System. A similar set of experiments was carried out with TiB_2 as was done with TiC. Three types of boron were compared, the size and purity of which are shown in Table 1. The first sample was made with crystalline boron, B-1, the second sample with an amorphous boron, B-2, and the third sample with an extremely fine, submicrometer, amorphous boron, B-3. In all of the TiB_2 experiments, only the Ti-1 titanium was used.

Secondary electron micrographs of the boron precursors are shown in Figure 8. A micrograph of the titanium powder (Figure 8A) is included for size comparison. The crystalline boron (Figure 8B) consists of irregular polyhedra with a size range of 10–30 μm. The larger amorphous boron (Figure 8C) is similar, but has a finer particle size. There are a few particles with 5–10 μm size but the majority of particles are less than 5 μm. The submicrometer amorphous boron is rounded, with an approximate diameter of 0.1 μm. The fine particles agglomerate (Figure 8D) in a manner similar to the carbon black with an agglomerate size of 10–30 μm.

The overall appearance and characteristics of the CSF TiB_2 samples were similar to those of the CSF TiC. The melting point, adiabatic reaction temperature, and standard heat of formation for TiC and TiB_2 are shown in Table 4. As can be seen, the melting points of both are about 3,200 K. A significant difference between them is the fact that both reactants melt (T_m(Ti) = 1,940 K, T_m(B) = 2,570 K) during the TiB_2 reaction, but not during the TiC reaction (T_{sub}(C) = 3,950 K). Consequently, it would not be surprising if this difference is reflected in the sample microstructure. Figure 9 shows both secondary and backscattered electron micrographs of representative areas of the CSF TiB_2 samples with the crystalline boron in Figures 9A and 9D, the larger amorphous boron in Figures 9B and 9E, and the submicrometer amorphous boron in Figures 9C and 9F. The carbon-like exoskeletons that were seen in the TiC products are absent in the CSF TiB_2 products. Instead, the samples consist of generally similarly shaped grains and the individual grains scale with the precursor boron size.

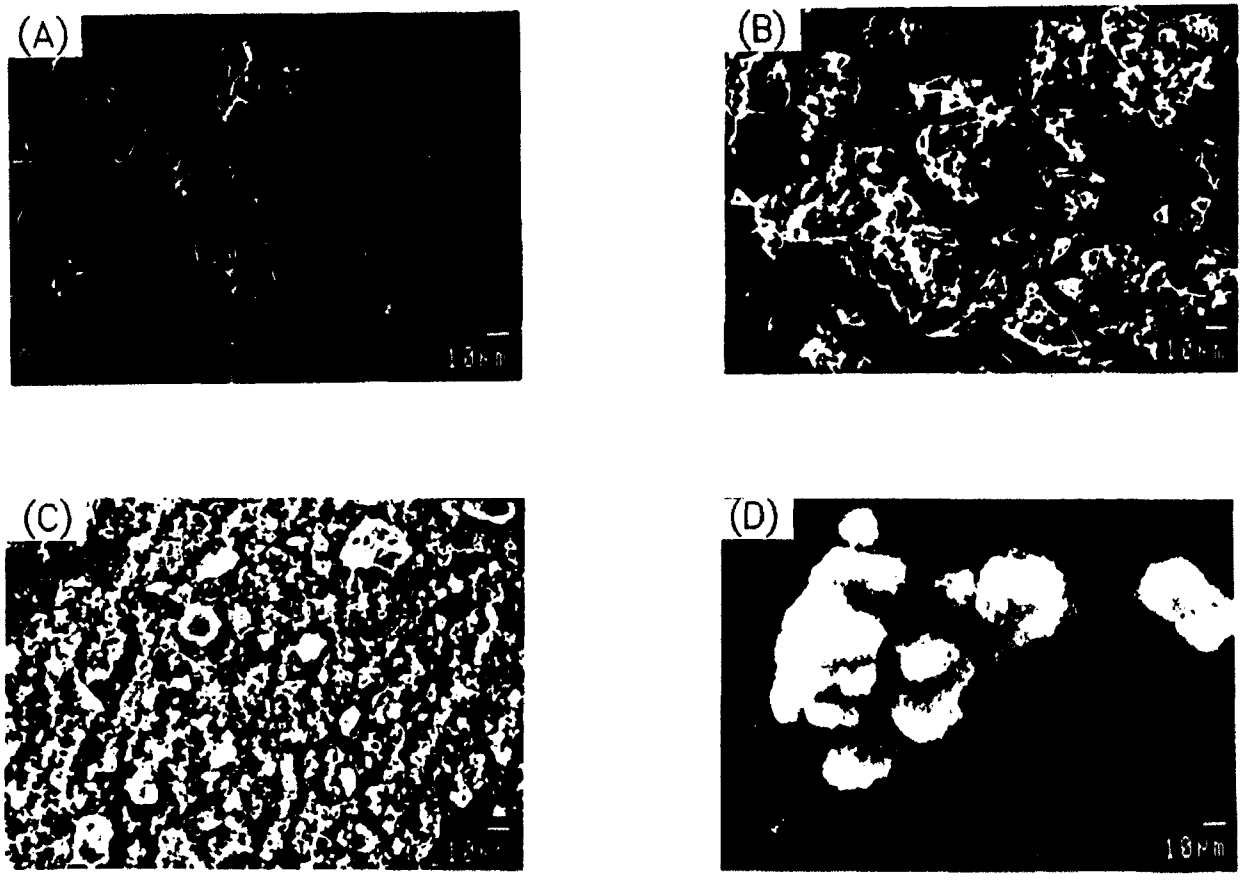

Figure 8. Secondary electron micrographs of the precursors powders with Ti-1 in 8A, B-1 crystalline boron in 8B, B-2 amorphous boron in 8C, and B-3 amorphous boron in 8D.

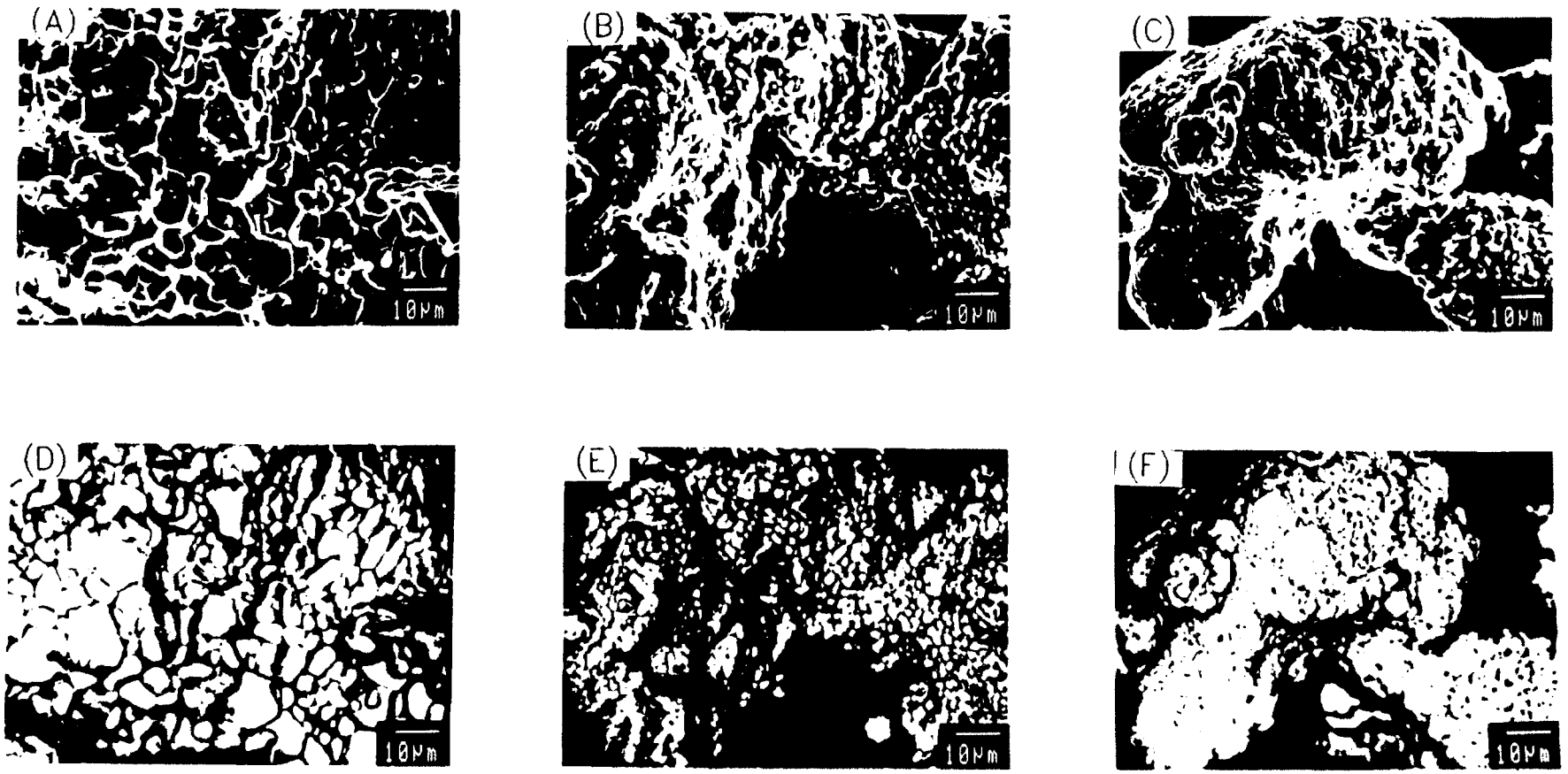

Figure 9. Secondary and backscattered electron images of the CSF TiB_2 products with the crystalline boron sample in 9A and 9D, the amorphous boron sample in 9B and 9E, and the submicrometer amorphous boron sample in 9C and 9F.

Table 4. TiC and TiB_2 Reaction Parameters

Parameter	TiC	TiB_2
T_m(K)	3,290	3,190
T_{ad}(K)	3,210	3,190
H_f^{298}(kJ/mole)	−184.0	−324.0

The morphology of the grains contained in the aggregates can be explained once the sample fragments are dispersed, mounted, and polished. Polished cross sections of CSF fragments, shown in Figure 10, reveal that each grain is a single crystal of TiB_2 with a hexagonal crystal structure. As seen in Figure 10A, the size of crystals with crystalline boron is about 5–10 μm. In Figures 10B and 10C, the samples with amorphous boron, the crystal size is smaller, 2–10 μm and 1–4 μm, respectively. The use of amorphous boron affects the interior porosity of the fragments as well. In addition to the larger, 10–30 μm, closed pores found in all of the samples, samples with amorphous boron also contain a secondary micrometer-sized porosity. These much smaller, closed pores are spread throughout the aggregates and appear between individual crystals. This fine porosity is most likely caused by the larger amount of trapped volatile impurities on the much larger surface area of the B-3 amorphous boron precursors.

The results of the second set of experiments, CSC, with boron, are shown in Figure 11. Backscattered electron images of polished and fracture surfaces with crystalline boron appear in Figures 11A and 11D, the larger amorphous boron in Figures 11B and 11E, and the submicrometer amorphous boron in Figures 11C and 11F. The figures show that these TiB_2 structures contain randomly oriented, hexagonal single crystal grains. The definite dependence of crystal size upon boron type, observed in the CSF samples, is absent. The CSC products consist of similarly sized 10–20 μm crystals. The porosity in these samples with crystalline and larger amorphous borons remains about the same as that of the CSF samples. The porosity in the sample with the submicrometer amorphous boron is, however, significantly different. The disappearance of the finer intergrain porosity seen in Figure 10 for the CSF samples is likely related to the considerable grain growth caused by the slow cooling and, consequently, enhanced sintering of the CSC product in the reaction fixture.

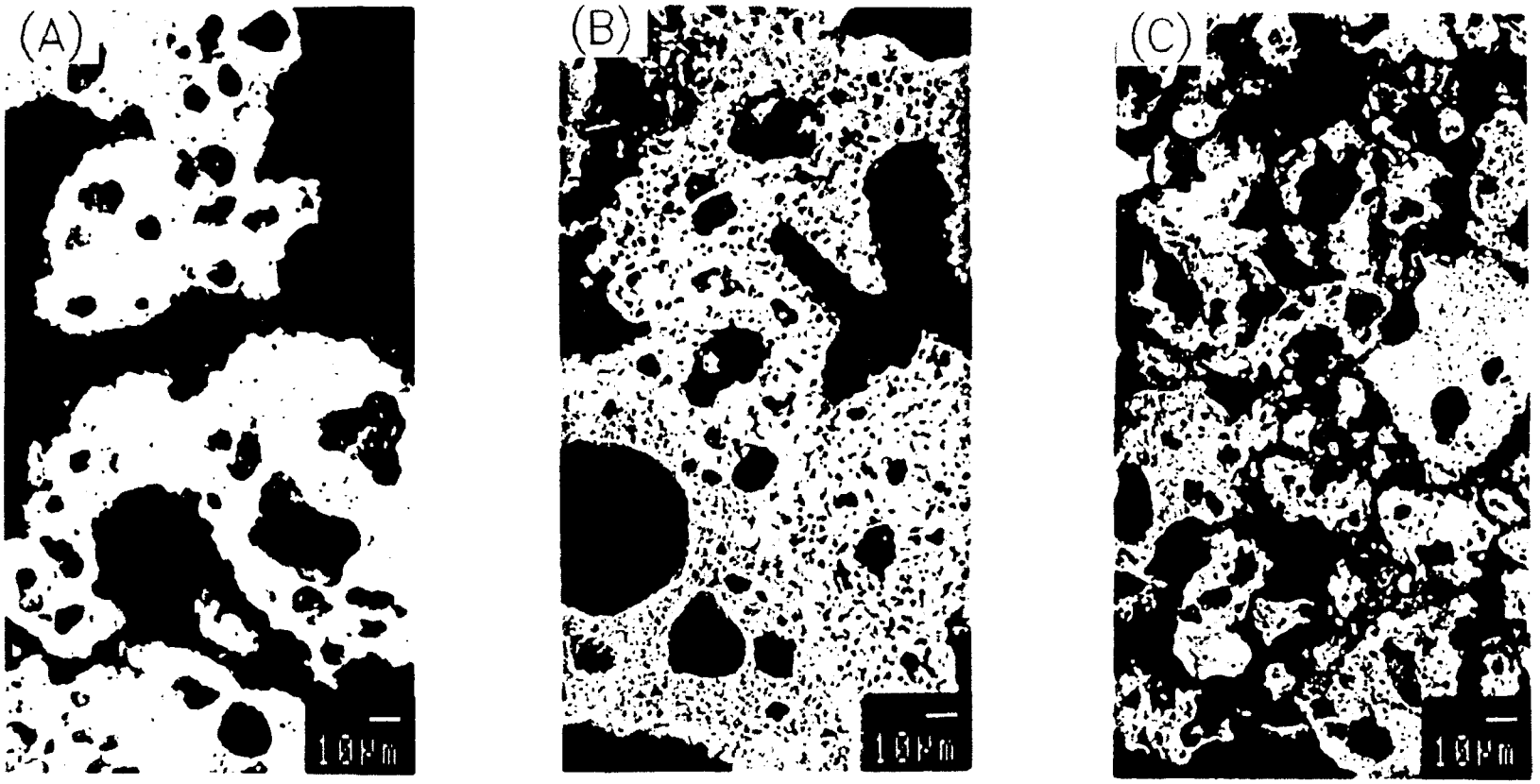

Figure 10. Backscattered electron micrographs of polished cross sections of the CSF powdered TiB_2 products. The crystalline boron sample is shown in 10A, amorphous boron sample in 10B, and the submicrometer amorphous boron sample in 10C.

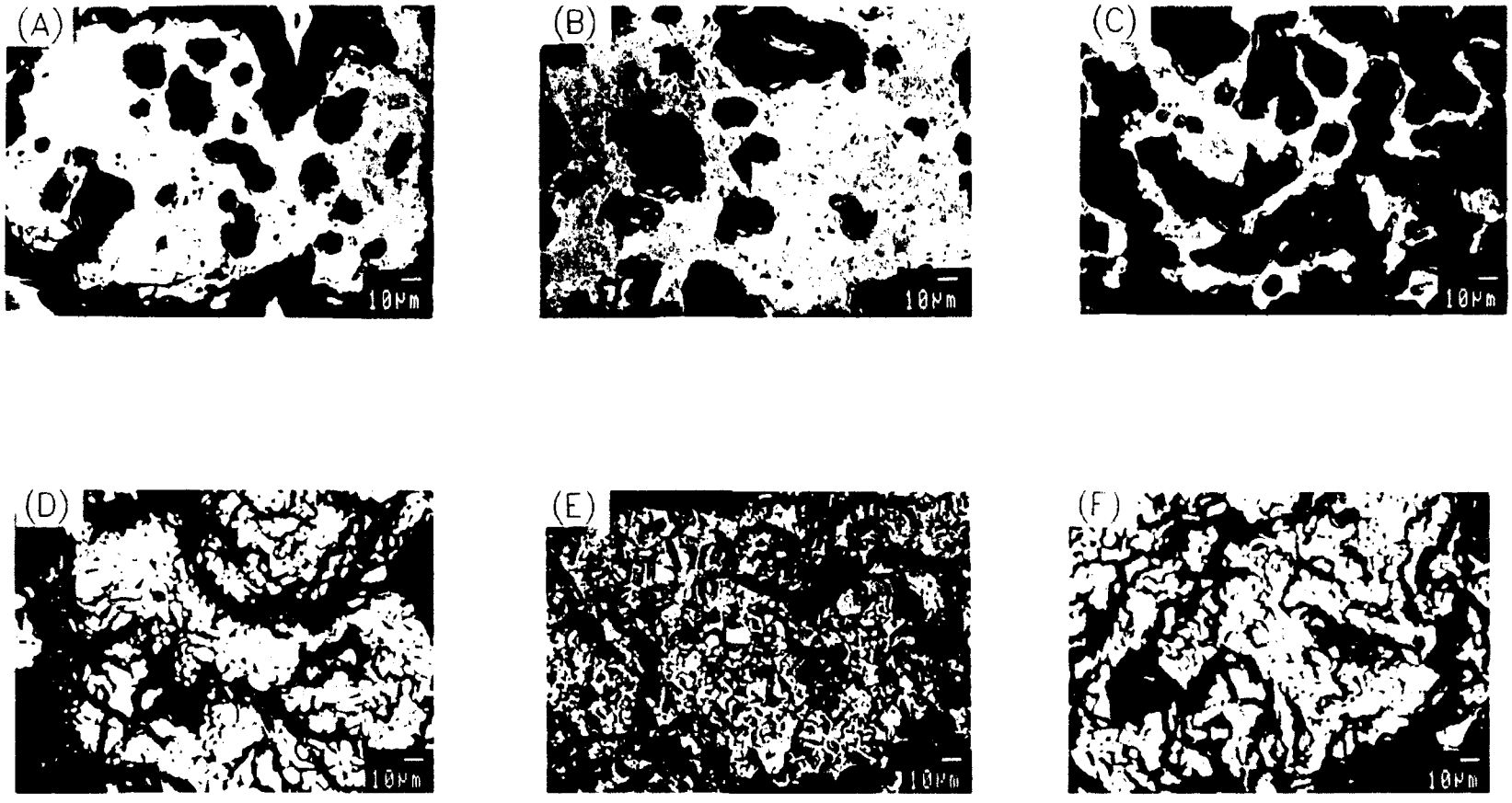

Figure 11. Polished and fracture surfaces of the CSC TiB_2 samples. The crystalline boron sample is shown in 11A and 11D, the amorphous boron sample in 11B and 11E, and the submicrometer amorphous boron sample in 11C and 11F.

Analysis of the CSDC TiB_2 structures reveals trends similar to those already identified in the CSF and CSC samples. Typical micrographs of polished and fracture surfaces are shown in Figure 12 with crystalline boron in Figures 12A and 12D, the larger amorphous boron in Figures 12B and 12E, and the submicrometer amorphous boron in Figures 12C and 12F. Again, the CSDC structures show the presence of the TiB_2 crystals. Although the crystal size is generally similar among the samples, much like the effect found with TiC earlier, there is a slight decrease caused by the difference in precursor purity. (See Table 5.) An aspect of the grain morphology not reflected in the table but evident in the micrographs is the fact that, in general, the TiB_2 crystals are not equiaxed. The polished cross sections indicate a definite increase in the residual porosity with the use of finer amorphous boron. From the number of transgranular fracture sites, it may be concluded that better intergrain bonding exists in the sample with crystalline boron, i.e., the sample with the least porosity. As seen in Table 6, another consequence of the increasing residual porosity is the decreasing microhardness of the CSDC TiB_2 samples. In fact, the overall sample microhardness of the sample made with the submicrometer amorphous boron is only 50% of that of the sample with crystalline boron.

The increasing porosity of the samples with decreasing boron size can be attributed to two basic characteristics of combustion synthesis reactions. In the first, the self-purifying nature of the combustion synthesis event causes the evolution of volatiles trapped on the precursors. In the second, due to the increased surface contact between particles, reactions with finer precursor powders will have higher reaction rates. The combination of increased reaction rate and the expulsion of trapped volatiles results in a quite violent CS reaction that sometimes disrupts and breaks up the reacting sample. Thus, the use of very small grain size amorphous boron can result in the undesirable combination of these two factors.

The reaction of titanium and boron is somewhat less complex than the titanium and carbon reaction. Both components melt, intermix, and react in the reaction zone to form TiB_2. Once the TiB_2 crystals nucleate, they precipitate out of this melt. It is believed that the melting of both components causes the titanium and boron reaction to be more rapid and thus more violent. The heat losses imposed by the various containment fixtures used in these experiments coupled with the level of impurities on the precursors, explains the resultant TiB_2 product structures. In the case of the CSF powders, both the rapid heat loss and the evolution of volatile impurities cause the samples with finer boron to result in smaller grain sizes. For the samples reacted in the reaction/compaction fixture, the effect of the expulsion of impurities is still present. However, due to improved thermal insulation, heat loss in the reaction fixture

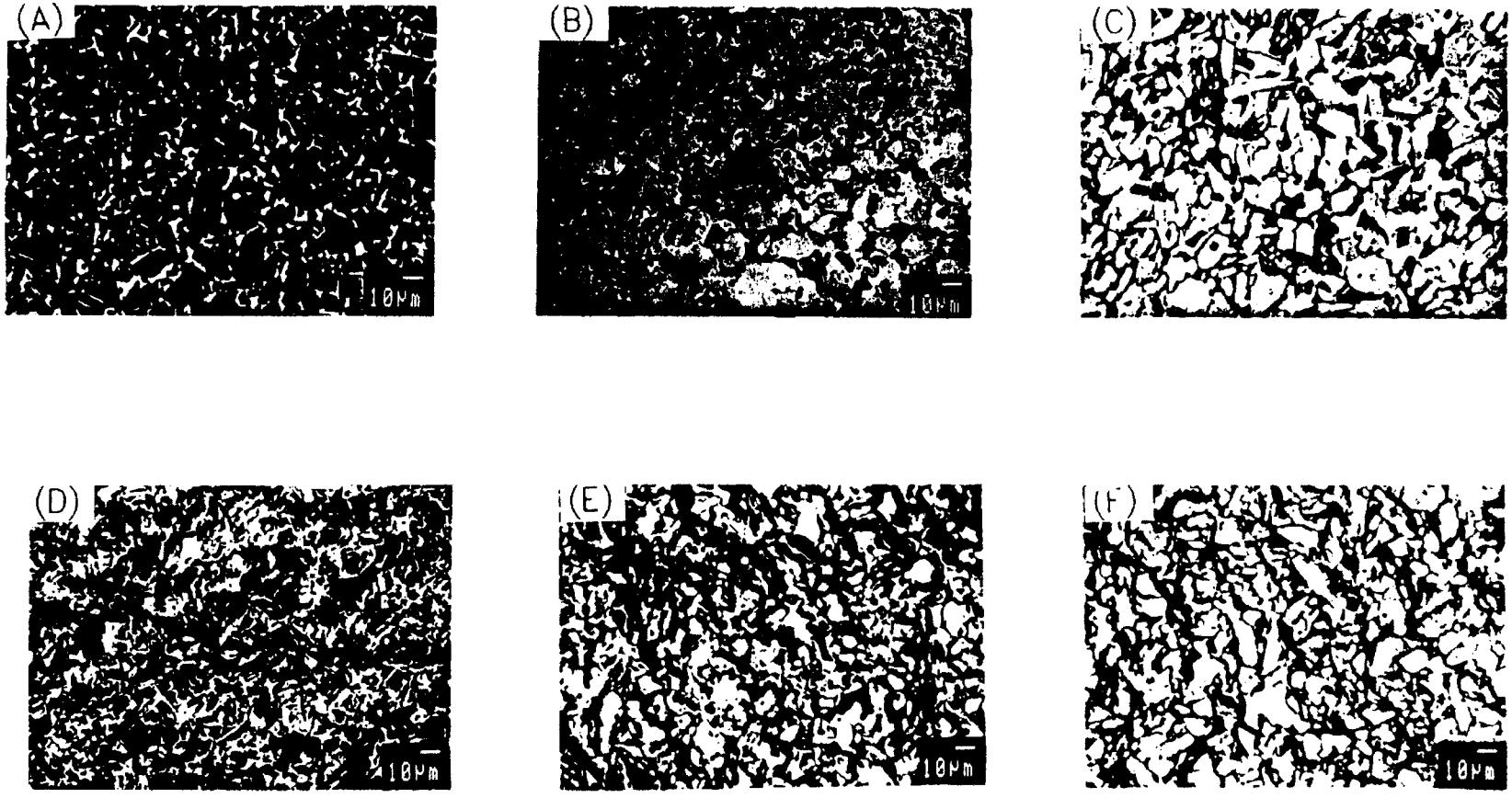

Figure 12. Polished and fracture surfaces of the CSDC TiB_2 samples. The crystalline boron sample is shown in 12A and 12D, the amorphous boron sample in 12B and 12E, and the submicrometer amorphous boron sample in 12C and 12F.

Table 5. TiB_2 Sample Grain Size

Sample	Precursors		No. of Grains	Grain Area, (μm^2)
TiB_2-1	Ti-1	B-1	255	130.0
TiB_2-2	Ti-1	B-2	251	70.0
TiB_2-3	Ti-1	B-3	214	90.0

Table 6. TiB_2 Sample Microhardness

Sample	Precursors		HK (100 g), (GPa)	HK (400 g), (GPa)
TiB_2-1	Ti-1	B-1	32.4+/–1.4	23.0+/–0.8
TiB_2-2	Ti-1	B-2	24.5+/–0.6	15.3+/–0.7
TiB_2-3	Ti-1	B-3	18.6+/–1.0	10.0+/–0.3

is greatly reduced. Therefore, over the long cooling period of the CSC samples, grain growth can take place, causing the elimination of some fine trapped pores. Finally, as was observed with TiC, in the dynamically consolidated TiB_2 samples, it is believed that the consolidation serves to close out the residual porosity from the bulk. If the residual porosity is too extensive, as is the case with fine boron, the effectiveness of the consolidation is limited.

4. CONCLUSIONS

Experiments were designed to determine the effect of the use of precursors with different morphologies and purities on three fabrication processing steps to produce TiC and TiB_2 ceramics. In all three stages, the characteristics of the precursor carbon and boron morphologies were found to influence the product's general characteristics and microstructure. While the type of the precursor had little or no bearing on the underlying product grain shape or morphology, its purity was found to have a significant role on the overall product structure. Specifically, all TiC samples consisted of equiaxed polyhedral

grains, and all TiB_2 samples consisted of hexagonal single crystal grains. However, the variation of product grain size with solid impurity concentration was found to be as much as an order of magnitude. Similarly, the residual porosity and degree of intergrain bonding in the CSF and CSC products were strongly dependent on the levels of volatile impurities in the precursors.

In the titanium-carbon system, the carbon precursor morphology affected the product morphology only when the reactants were unconstrained. Whereas the exterior surface of the CSF products was found to mimic the precursor carbon shape, the actual interior grain structure was independent of the type of carbon and is believed to be determined by other factors. Due to improved thermal insulation and spatial constraint in the confines of the reaction vessel, morphology differences in the CSC samples became less pronounced. These differences were caused by the impurities found on the precursors and influenced the degree of intergrain bonding and the level of residual closed porosity. With the imposition of dynamic consolidation, any morphological differences remaining in the CSC samples were eliminated. In cases where the intermediate CSC structure retained a high degree of porosity, some of the morphological differences could not be entirely eliminated during consolidation.

In the titanium-boron system, the combustion synthesis reaction involves the melting of both components, which results in the formation of a melt, nucleation, and subsequent precipitation of TiB_2 crystals. The nucleation of the TiB_2 crystals occurs during or soon after the combustion synthesis reaction. Comparisons of the CSF and CSC products revealed that the precipitation process was unaffected by the geometrical constraints imposed by the reaction fixture. The fixture provided a well-insulated environment for grain growth to occur. The type of boron was found to influence the residual porosity of all three types of TiB_2 samples. When finer boron powders are used, the expulsion of volatile impurities is so violent that dynamic consolidation alone could not eliminate the porosity of the CSC samples.

In these experiments, it has been shown that the underlying grain morphology of CS/DC TiC and TiB_2 is independent of the type of precursor used in their fabrication. However, the structural and mechanical integrity of these ceramics were observed to be very much dependent on the initial conditions of the precursors as well as on their handling during the various processing stages. Consequently, the development and evolution of the CS/DC product and its intermediate structures could be easily compromised without care in the selection and treatment of the precursors.

5. REFERENCES

Adachi, S., T. Wada, T. Mihara, Y. Miyamoto, M. Koizumi, and O. Yamada. "Fabrication of Titanium Carbide Ceramics by High-Pressure Self-Combustion Sintering of Titanium Powder and Carbon Fiber." Journal of the American Ceramic Society, vol. 72, no. 5, pp. 805–809, 1989.

Dunmead, S. D., D. W. Readey, C. E. Semler, and J. B. Holt. "Kinetics of Combustion Synthesis in the Ti-C and Ti-C-Ni Systems." Journal of the American Ceramic Society, vol. 72, no. 12, pp. 2318–2324, 1989.

Kecskes, L. J., T. Kottke, P. H. Netherwood, Jr., R. F. Benck, and A. Niiler. "Explosive Consolidation of Combustion Synthesized TiB_2 and TiC: Microstructural Properties." BRL-TR-3133, U.S. Army Ballistic Research Laboratory, Aberdeen Proving Ground, MD, 1990.

Kecskes, L. J., T. Kottke, and A. Niiler. "Microstructural Properties of Combustion-Synthesized and Dynamically Consolidated Titanium Boride and Titanium Carbide." Journal of the American Ceramic Society, vol. 73, no. 5, pp. 1274–1282, 1990.

Kecskes, L. J., and A. Niiler. "A Study of Impurities in Combustion Synthesis Systems." BRL-MR-3658, U.S. Army Ballistic Research Laboratory, Aberdeen Proving Ground, MD, 1988.

Kottke, T., L. J. Kecskes, and A. Niiler. "Control of Titanium Diboride SHS Reactions by Inert Dilutions and Mechanical Constraint." Journal of the American Institute of Chemical Engineers, vol. 36, no. 10, pp. 1581–1584, 1990.

Mullins, M. E., and E. Riley. "The Effect of Carbon Morphology on the Combustion Synthesis of Titanium Carbide." Journal of Materials Research, vol. 4, no. 2, pp. 408–411, 1989.

Niiler, A., L. J. Kecskes, and T. Kottke. "Shock Consolidation of Combustion Synthesized Ceramics." Combustion and Plasma-Synthesis of High-Temperature Materials, Z. A. Munir and J. B. Holt, Editors, VCH Publishers, New York, NY, 1990.

Niiler, A., L. J. Kecskes, T. Kottke, P. H. Netherwood Jr., and R. F. Benck. "Explosive Consolidation of Combustion Synthesized Ceramics: TiC and TiB_2." BRL-TR-2951, U.S. Army Ballistic Research Laboratory, Aberdeen Proving Ground, MD, 1988.

Riley, M. A., and A. Niiler. "Low Pressure Compaction of SHS Prepared Ceramics." BRL-MR-3574, U.S. Army Ballistic Research Laboratory, Aberdeen Proving Ground, MD, 1987.

INTENTIONALLY LEFT BLANK.

No. of Copies	Organization
2	Administrator Defense Technical Info Center ATTN: DTIC-DDA Cameron Station Alexandria, VA 22304-6145
1	Commander U.S. Army Materiel Command ATTN: AMCAM 5001 Eisenhower Ave. Alexandria, VA 22333-0001
1	Director U.S. Army Research Laboratory ATTN: AMSRL-OP-CI-AD, Tech Publishing 2800 Powder Mill Rd. Adelphi, MD 20783-1145
2	Commander U.S. Army Armament Research, Development, and Engineering Center ATTN: SMCAR-IMI-I Picatinny Arsenal, NJ 07806-5000
2	Commander U.S. Army Armament Research, Development, and Engineering Center ATTN: SMCAR-TDC Picatinny Arsenal, NJ 07806-5000
1	Director Benet Weapons Laboratory U.S. Army Armament Research, Development, and Engineering Center ATTN: SMCAR-CCB-TL Watervliet, NY 12189-4050
(Unclass. only) 1	Commander U.S. Army Rock Island Arsenal ATTN: SMCRI-IMC-RT/Technical Library Rock Island, IL 61299-5000
1	Director U.S. Army Aviation Research and Technology Activity ATTN: SAVRT-R (Library) M/S 219-3 Ames Research Center Moffett Field, CA 94035-1000

No. of Copies	Organization
1	Commander U.S. Army Missile Command ATTN: AMSMI-RD-CS-R (DOC) Redstone Arsenal, AL 35898-5010
1	Commander U.S. Army Tank-Automotive Command ATTN: ASQNC-TAC-DIT (Technical Information Center) Warren, MI 48397-5000
1	Director U.S. Army TRADOC Analysis Command ATTN: ATRC-WSR White Sands Missile Range, NM 88002-5502
1	Commandant U.S. Army Field Artillery School ATTN: ATSF-CSI Ft. Sill, OK 73503-5000
(Class. only) 1	Commandant U.S. Army Infantry School ATTN: ATSH-CD (Security Mgr.) Fort Benning, GA 31905-5660
(Unclass. only) 1	Commandant U.S. Army Infantry School ATTN: ATSH-CD-CSO-OR Fort Benning, GA 31905-5660
1	WL/MNOI Eglin AFB, FL 32542-5000
	Aberdeen Proving Ground
2	Dir, USAMSAA ATTN: AMXSY-D AMXSY-MP, H. Cohen
1	Cdr, USATECOM ATTN: AMSTE-TC
1	Dir, ERDEC ATTN: SCBRD-RT
1	Cdr, CBDA ATTN: AMSCB-CI
1	Dir, USARL ATTN: AMSRL-SL-I
10	Dir, USARL ATTN: AMSRL-OP-CI-B (Tech Lib)

No. of Copies	Organization
2	Commander U.S. Army Foreign Science and Technical Center ATTN: Mr. J. F. Crider Mr. W. Marley 220 Seventh Street, NE Charlottesville, VA 22901
3	Commander Army Materials Technology Laboratory ATTN: AMXMR-OM, Dr. J. V. Marzik Dr. W. J. Croft AMXMR-MCP, Dr. D. Viechnicki Watertown, MA 02172
3	Commander U.S. Army Research Office ATTN: Dr. I. Ahmad Dr. A. Crowson Dr. R. Reeber P. O. Box 12211 Research Triangle Park, NC 27709
1	Defense Advance Research Project Agency ATTN: Dr. P. A. Parrish 3701 N. Fairfax Dr. Arlington, VA 22203-1714
3	Idaho Nat. Eng. Laboratory ATTN: Dr. G. E. Korth Dr. B. H. Rabin Dr. R. N. Wright P.O Box 1625 Idaho Falls, ID 83415
2	Director Lawrence Livermore National Laboratory ATTN: Dr. J. B. Holt, L-369 Dr. D. Maiden, MS-L71 P. O. Box 808 Livermore, CA 94550
4	Director Los Alamos National Laboratory ATTN: Dr. R. Behrens, MS-3C348 Dr. S. E. Caldwell Dr. D. Sandstrom, MS-G756 Dr. K. F. Wylie, MS-G780 P. O. Box 1663 Los Alamos, NM 87545
1	National Bureau of Standards ATTN: Dr. S. J. Schneider Room A257, Bldg. 223 Washington, DC 20234
1	Director Sandia National Laboratories Applied Mathematics Div. 8231 ATTN: Dr. S. B. Margolis Livermore, CA 94550
1	AIRTRON Division ATTN: Dr. J. Ings 200 East Hanover Ave. Morris Plains, NJ 07950
1	ALCOA Laboratory ALCOA Tech Center ATTN: Dr. A. J. Becker Alcoa Center, PA 15069
1	Battelle Metalworking Section ATTN: Dr. V. D. Linse 505 King Ave. Columbus, OH 43201-2693
1	California Institute of Technology ATTN: Dr. T. D. Vreeland Keck Laboratories, MS138-78 Pasadena, CA 91125
2	General Sciences, Inc. ATTN: Dr. P. D. Zavitsanos Dr. J. J. Gebhardt P. O. Box 185 Norristown, PA 10401

No. of Copies	Organization
3	Georgia Institute of Technology ATTN: Ms. K. V. Logan Mr. G. R. Villalobos Dr. J. D. Walton EES/EMSL Atlanta, GA 30332
1	Lockheed Palo Alto Research Laboratory ATTN: Dr. A. P. Hardt 3251 Hanover Street Palo Alto, CA 94304
3	Martin Marietta Laboratories ATTN: Dr. D. C. Nagle Dr. S. R. Winzer Mr. M. A. Riley 1450 South Rolling Road Baltimore, MD 21227
2	New Mexico Tech ATTN: Dr. N. Thadani Dr. P. A. Persson CETR Socorro, NM 87801
1	New Mexico Technology Materials/Metallurgical Engr. ATTN: Dr. O. T. Inal Socorro, NM 87801
1	New York State College of Ceramics ATTN: Dr. J. W. McCauley Alfred University Alfred, NY 14802
1	Rice University ATTN: Dr. J. Margrave P. O. Box 2692 Houston, TX 77252
3	State University of New York ATTN: Dr. V. Hlavacek Dr. J. Puszynski Dr. S. Majorowski Amherst Campus Furnas Hall 507 Buffalo, NY 14260

No. of Copies	Organization
1	Terra Tek, Inc. ATTN: R. A. Cutler 400 Wakara Way Salt Lake City, UT 84108
1	University of California College of Engineering ATTN: Dr. Z. Munir Davis, CA 95616
1	University of California, San Diego Department of Appl. Mechanics and Engineering Science ATTN: Dr. M. A. Meyers La Jolla, CA 92093
1	University of Delaware Department of Mechanical Engineering ATTN: Dr. I. W. Hall Newark, DE 19717

No. of
Copies Organization

1 Government Industrial Research Institute
Tohoku
ATTN: Dr. N. Sata
4-5-1 Nigatake
Miyagino-ku
Sendai Miyagi 983, JAPAN

1 National Research Institute for Metals
ATTN: Dr. Y. Kaieda
2-3-12 Nakameguro
Meguro-ku
Tokyo 153, JAPAN

1 Osaka University
ATTN: Dr. Y. Miyamoto
Ibaraki
Osaka 567, JAPAN

1 Ryukoku University
ATTN: Dr. M. Koizumi
1-5 Yokoya, Oe-cho,
Otsu Shiga 520-21, JAPAN

2 Tokyo Institute of Technology
ATTN: Dr. A. Sawaoka
Dr. O. Odawara
4259 Nagatsuata
Midori-ku
Yokohama 227, JAPAN

USER EVALUATION SHEET/CHANGE OF ADDRESS

This Laboratory undertakes a continuing effort to improve the quality of the reports it publishes. Your comments/answers to the items/questions below will aid us in our efforts.

1. ARL Report Number ARL-TR-107 Date of Report April 1993

2. Date Report Received _____

3. Does this report satisfy a need? (Comment on purpose, related project, or other area of interest for which the report will be used.) _____

4. Specifically, how is the report being used? (Information source, design data, procedure, source of ideas, etc.) _____

5. Has the information in this report led to any quantitative savings as far as man-hours or dollars saved, operating costs avoided, or efficiencies achieved, etc? If so, please elaborate. _____

6. General Comments. What do you think should be changed to improve future reports? (Indicate changes to organization, technical content, format, etc.) _____

CURRENT ADDRESS

_____
Organization

_____
Name

_____
Street or P.O. Box No.

_____
City, State, Zip Code

7. If indicating a Change of Address or Address Correction, please provide the Current or Correct address above and the Old or Incorrect address below.

OLD ADDRESS

_____
Organization

_____
Name

_____
Street or P.O. Box No.

_____
City, State, Zip Code

(Remove this sheet, fold as indicated, staple or tape closed, and mail.)

DEPARTMENT OF THE ARMY

OFFICIAL BUSINESS

BUSINESS REPLY MAIL
FIRST CLASS PERMIT No 0001, APG, MD

Postage will be paid by addressee

Director
U.S. Army Research Laboratory
ATTN: AMSRL-OP-CI-B (Tech Lib)
Aberdeen Proving Ground, MD 21005-5066

NO POSTAGE
NECESSARY
IF MAILED
IN THE
UNITED STATES